CME LIVE OPEN ACCESS

Journal of
Applied Mechanics Reviews and Reports

Research Article

ISSN: 3069-0803

FEA Based Biomechanical Analysis of Stainless Steel and Magnesium Alloy Femur Bone Plates Under Healing-Stage Load Conditions

M M Tariqul Islam Mesbah*, Md Tanvir Shahariar and Abdullah-Al-Mamun

Department of Mechanical Engineering, Chittagong University of Engineering & Technology (CUET), Chattogram-4349, Bangladesh.

Corresponding Author: M M Tariqul Islam Mesbah, Department of Mechanical Engineering, Chittagong University of Engineering & Technology (CUET), Chattogram-4349, Bangladesh.

Received: 2026 Jun 06 **Accepted:** 2026 Jun 29 **Published:** 2026 July 22

Abstract

Bone plates are widely used to stabilize femur fractures, but selecting the right material and design remains a challenge. This study presents a comparative finite element analysis (FEA) of two common plates—Dynamic Compression Plate (DCP) and Locking Compression Plate (LCP)—made from stainless steel and biodegradable magnesium alloy. To improve realism, a patient-specific femur model was used instead of a simplified geometry. A fractured femur with a small gap was modeled, and the plate–bone system was analyzed under static loading. Loads from 140 N to 700 N were applied to represent increasing weight-bearing during healing for a 70 kg person. In this study, healing stages were represented only through increasing load; changes in bone structure or material properties during healing were not modeled. For simplicity, screw geometry was not included, and bonded connections were used. The results show that stainless steel plates remain within safe stress and deformation limits (<160 MPa, <1.6 mm) even at higher loads, making them suitable for full weight-bearing. In contrast, magnesium plates show higher stress and deformation, exceeding their strength at higher loads. This suggests a risk of failure in adults but potential use in low-load cases, such as early healing or pediatric patients. Although the results follow expected material behavior, this study provides a clear comparison using realistic geometry and clinically relevant loading. Future work should include more detailed modeling and experimental validation.

Keywords: *Finite Element Analysis, Orthopedic Plates, Stainless Steel, Magnesium Alloy, Bone Healing Stages*

1. Introduction

The coordinated interplay between muscles and bones is fundamental to human motion, with muscles (comprising nearly 50% of body mass) generating forces that are transmitted through the skeleton to enable movement, posture, and protection. Among the 206 bones in the human body, the femur stands out as the longest and strongest (Fig. 1), bearing the majority of body weight and playing a crucial role in locomotion [1]. Despite its robustness, the femur is susceptible to fractures caused by high-energy impacts, such as vehicular accidents or sports injuries, and even minor trauma in osteoporotic individuals. Stabilization of such fractures often requires orthopedic implants like bone plates, which serve to realign and secure fractured segments, facilitating effective healing. Conventional bone plates, typically made from titanium or stainless steel, are favored for their durability, biocompatibility, and mechanical stability throughout the healing process [2]. Two commonly used plates are the Dynamic Compression Plate (DCP) and the Locking Compression Plate (LCP) (Fig. 1). DCPs function by applying compressive forces across the fracture site using eccentrically placed screws, thereby promoting direct bone healing, while LCPs utilize locking screws that enhance angular stability and are particularly suited for complex or osteoporotic fractures [3]. The material choice for these implants is critical; non-biodegradable metals like stainless steel and titanium provide long-term structural support, whereas biodegradable alternatives, such as magnesium alloys, offer the advantage of gradual in vivo degradation, eliminating the need for secondary removal surgeries [4]. However, magnesium alloys face challenges related to rapid corrosion and hydrogen gas evolution, necessitating further optimization. Fracture healing itself is a multistage process comprising the inflammatory phase (hematoma formation and cellular recruitment), soft callus formation (cartilage development), hard callus formation (woven bone replacement), and remodeling (mature lamellar bone restoration) (**Fig. 1**), each with distinct biomechanical demands on the implant [5]. Therefore, both implant design and material selection must align with the evolving mechanical environment of the healing femur.

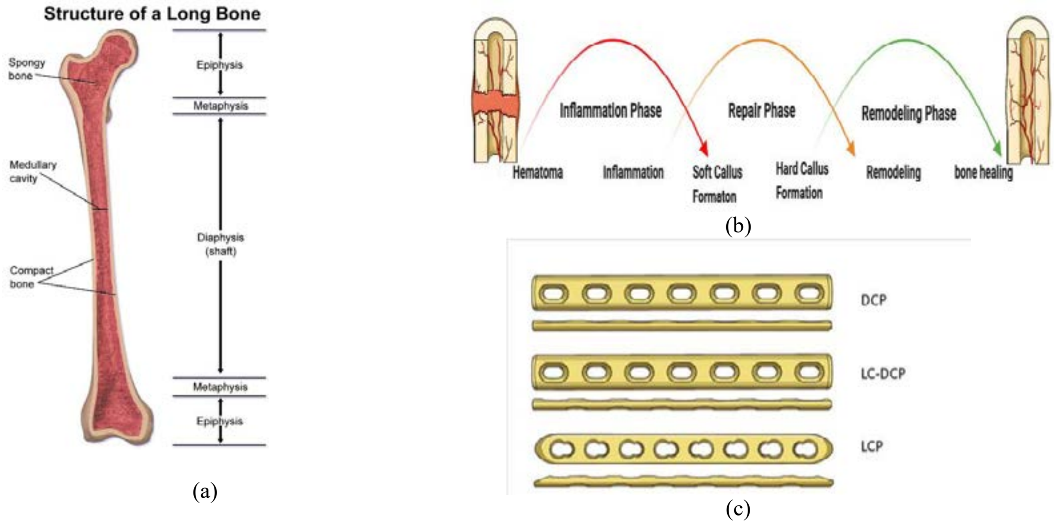

Figure 1: (a) Structure of Long Bone [6] (b) Schematic Summary of the Stages of Bone Healing [7] (c) Bone Plates type Based on Structure [8]

The femur, extending from the hip to the knee, is the longest and strongest bone in the human body, structurally adapted to support extensive muscular and ligamentous attachments essential for locomotion, weight-bearing, and stability [9]. Anatomically, it is divided into the proximal region (comprising the femoral head, neck, and trochanters for hip articulation), the shaft (curved for optimal stress distribution during walking and running), and the distal end (which interacts with the patella and tibia to form the knee joint). The femur's composition includes two primary bone tissues: cortical (compact) bone forming 80% of the skeleton and providing resistance to bending and torsion, and cancellous (trabecular) bone within the medullary cavity that aids in localized load distribution [10]. Despite its strength, the femur is vulnerable to fractures from high-energy trauma or, in osteoporotic individuals, even minor falls. Femoral fractures disrupt mobility, functional independence, and often result in extended recovery, especially among the elderly [11]. To restore anatomical alignment and facilitate healing, internal fixation using bone plates is a common clinical intervention. These thin, high-strength devices, typically made from stainless steel or titanium—are affixed to the bone using screws to stabilize and support healing under mechanical loads [2]. Several types of bone plates are used depending on fracture complexity and location. Structurally, Dynamic Compression Plates (DCPs) apply controlled compression across the fracture via eccentric screw placement, enhancing stability and alignment.

Locking Compression Plates (LCPs), designed with locking screws, offer angular stability and are particularly useful for osteoporotic or comminuted fractures due to minimal disruption of periosteal blood flow. The Limited Contact DCP (LC-DCP) further improves healing by reducing vascular damage through a minimized contact profile [12]. Materials also influence clinical outcomes. Stainless steel plates offer high durability but may cause stress shielding, while titanium alloys provide lower weight, superior biocompatibility, and corrosion resistance. Cobalt-chromium alloys exhibit excellent wear resistance but may introduce rigidity issues. Magnesium alloys, emerging as third-generation biomaterials, are lightweight, biodegradable, and osteoconductive, reducing stress shielding and eliminating the need for implant removal. However, their rapid degradation and hydrogen gas release remain challenges [13]. Bone healing occurs in overlapping stages: inflammation, repair (soft and hard callus), and remodeling. Initially, a hematoma forms, initiating cellular recruitment and inflammation [14]. This is followed by the formation of a fibrous-cartilaginous soft callus, which later mineralizes into a hard callus of woven bone. Over time, the bone remodels into mature lamellar bone, regaining its original mechanical properties [15]. Each healing phase presents unique biomechanical demands, underscoring the importance of selecting implants that support both biological and mechanical aspects of fracture recovery across the full healing timeline. Bone plates have long served as essential orthopedic implants for stabilizing fractures across various anatomical sites, including the femur, which is particularly critical due to its role in weight-bearing and mobility. The choice of bone plate design and material is influenced by several factors including fracture type, anatomical site, mechanical demands, and healing objectives [16]. Historically, the use of internal fixation was pioneered by Hansmann in the late 19th century, and later revolutionized by the AO Foundation in 1958, setting the groundwork for standardized bone plate design and application [17]. Initial generations of bone plates, such as those by Lane and Lambotte, were marred by complications like corrosion and mechanical insufficiency. To counter these issues, Dynamic Compression Plates (DCPs) and Limited Contact-DCPs (LC-DCPs) were introduced, offering improved mechanical fixation but introducing drawbacks like stress shielding and cortical thinning.

This evolution led to the development of compressible and biodegradable plates, promoting micromotion and enhancing bone healing [18]. With the advancement of computational tools, Finite Element Analysis (FEA) has become instrumental in evaluating biomechanical performance. Ahirwar et al. used FEA to analyze femur bones (both isotropic and anisotropic) and different biomaterials (SS 316L, Ti-6Al-4V, and Co-Cr), identifying SS 316L and Ti-6Al-4V as optimal choices due to reduced interface stress and improved deformation response. Their study also highlighted the benefits of double plate fixation for better load distribution and minimized stress shielding [19]. Miguel Marco et al. combined XFEM simulations and experimental validation to understand early-stage femoral fracture mechanisms, stressing the importance of accurate bone material characterization for realistic simulations [20]. Similarly, Ganesh et al. proposed stiffness-graded plates (SGPs) as biomechanically superior to traditional stainless-steel plates (SSPs), since SGPs enhance compressive stress at the fracture site while preserving tensile stress along the bone, mitigating stress shielding and facilitating better healing [21]. In further FEA-based studies, Kalaiyarasan et al. examined the mechanical behavior of femoral fractures using Al8090 and SiC, determining higher stress concentration in the midshaft and maximum deformation at the femoral head, thus supporting the application of alternative biomaterials for enhanced durability [22]. Likewise, Coquim and team analyzed midshaft femur defects and found that a lateral plate with medial strut and maximal screw usage provided the greatest structural stiffness [23]. To explore alternative materials, Bagheri et al. evaluated a CF/Flax/Epoxy composite plate for femur fractures, which demonstrated comparable stiffness to metal plates but with reduced stress shielding, indicating better biomechanical compatibility [24]. Amalraju and Dawood also showed that titanium plates outperformed SS 316L in terms of lower stress and displacement, attributing it to titanium's high strength-to-weight ratio, corrosion resistance, and biocompatibility [25]. Dhanopia and Bhargava assessed PMMA thermoplastic plates, which effectively reduced stress concentrations and deformation, presenting a low-cost and stable solution for femoral fracture management [26]. Another comparative FEA study by Sankar et al. highlighted titanium as the best material among SS, Alumina, Nylon, and PMMA due to its ability to limit equivalent stress and deformation under eccentric loading [27]. In terms of material optimization, Satapathy et al. investigated functionally graded materials (FGMs) made of titanium and hydroxyapatite, revealing a 63% increase in stress at the fracture site and a 15% reduction in deformation. This enhanced performance is particularly beneficial under torsional loading [28].

Fouad's study further confirmed FGMs' superiority by showing reduced stress shielding under torsional and axial loads, and better stimulation of healing due to the minimization of interfacial gaps [29]. For complex comminuted distal femur fractures, Guo et al. employed a dual-plate system with promising clinical results, achieving an average bone union time of 5.4 months, though complications such as infection were observed [30]. On a broader biological scale, Ferrucci et al. linked aging-related osteoporosis and sarcopenia through biomechanical and biochemical pathways, suggesting that bone-muscle interactions significantly impact implant performance and healing [31]. Recent advancements have emphasized bioactive and biodegradable materials such as magnesium alloys and porous tantalum. These alternatives aim to reduce stress shielding, promote biological integration, and avoid secondary surgeries, despite challenges like rapid corrosion [32]. Amukarimi et al. reviewed efforts to improve the corrosion resistance of Mg-based implants, aiming to expand their orthopedic and vascular applications [4]. In biodegradable composite development, Mehboob et al. compared BGF/PLA and Mg/PLA composites with SS plates, noting superior mechanical performance and tissue differentiation in fluoride-coated Mg/PLA scaffolds due to their slower degradation and better stiffness [33]. Computational studies by Alaneme et al. validated the role of FEA in implant design optimization, highlighting its potential to predict mechanical and biodegradation behavior, thereby reducing prototyping costs and increasing implant safety [34]. Wicaksono et al. experimentally evaluated AZ31B magnesium plates under bending loads, concluding that plate geometry significantly affects stress distribution-DCP Broad Plates performed better than DCP Straight Plates due to more efficient stress handling [35]. Finally, Liebl et al. demonstrated the predictive power of FEA using in-vitro and in-vivo MDCT data, showing strong correlation with strain measurements and highlighting its clinical potential in fracture risk prediction [36].

To bridge the gaps in research, the present study employs anatomically accurate, patient-specific femur models combined with finite element simulations to assess the performance of DCP and LCP plates made from both stainless steel and magnesium alloys. Physiological loads corresponding to the four healing stages (140 N to 700 N) are applied to simulate a 70 kg adult in a standing posture. The analysis includes stress distribution and total deformation, providing a holistic understanding of the mechanical viability of each plate-material combination during healing. This study not only emphasizes the need for material innovation in orthopedic implant design but also reinforces the importance of incorporating anatomical realism and healing-phase specificity in simulation-based evaluations. The findings aim to support clinical decision-making by identifying the most appropriate implant strategies for diverse patient populations and healing scenarios.

2. Research Methodology

The quality and reliability of a research study depend heavily on the soundness of its methodological framework. This study integrates geometric modeling using SOLIDWORKS and finite element analysis (FEA) via ANSYS to assess the biomechanical performance of two bone plate designs-Dynamic Compression Plate (DCP) and Locking Compression Plate (LCP)-under physiological loading conditions across different stages of femur fracture healing.

2.1. Physical Modeling

Bone dimensions vary widely due to factors like individual anatomy, age, bone density, and overall structure, making it impossible to define them universally. In this study, the femur bone wasn't manually designed in SOLIDWORKS. Instead, it was imported from GrabCAD, a trusted source that offers CAD models created from CT scan data of real bones. This approach ensures that the CAD model's dimensions and structural details closely match those of an anatomically accurate femur, improving the reliability of the study's simulations and analyses.

2.1.1. Bone Import

A complete and anatomically accurate femur bone model was obtained from the GrabCAD [37] repository in the form of a CAD file. The model was subsequently imported into SOLIDWORKS for further processing, which included rendering and making necessary modifications to ensure compatibility with the specific requirements of the study. These modifications involved refining the geometric details, ensuring dimensional accuracy, and preparing the model for subsequent finite element analysis. The rendered and modified model is illustrated in Fig. 2 for reference.

2.1.2. Fracture Illustration

In real-life fracture cases, the bone tissue is likely to be in a much worse physical condition than normal bone. In making the computational analysis simple but related to real clinical conditions, the femur bone was modeled and divided into two regions: the upper and the lower section (see Fig. 2).To show fracture for facilitate analysis a gap of 1 mm (see Fig. 2) was provided between any two sections in SOLIDWORKS, as the fracture gaps usually reported range from 0.5 to 3 mm [38]. The gap dimension was purposely selected to model incomplete fractures with closely aligned bone fragments deliberated on partial fractures. Such a configuration permits a fitting simulation of the biomechanical behaviors under these conditions while remaining light on the computation.

2.1.3. Bone Plate Design

A 4.5 mm Dynamic Compression Plate (DCP) was selected, while a T-shaped Locking Compression Plate (LCP) with hole diameters of 4.5 mm and 5 mm was chosen. The "4.5 mm" specification refers to the hole diameter of the plate, which is an essential factor for accommodating screws of corresponding sizes. Detailed dimensions for both plates [39] are illustrated in the Fig. 2(all dimensions in mm). T-shaped locking plate incorporates two distinct hole diameters: one measuring 4.5 mm and the other 5 mm. The whole design was done in SOLIDWORKS. These variations in hole sizes are designed to optimize fixation and ensure compatibility with different screw types, ultimately enhancing the mechanical stability of the construct. This selection was made based on clinical relevance and established standards for orthopedic fixation devices, ensuring the finite element model accurately represents real world scenarios.

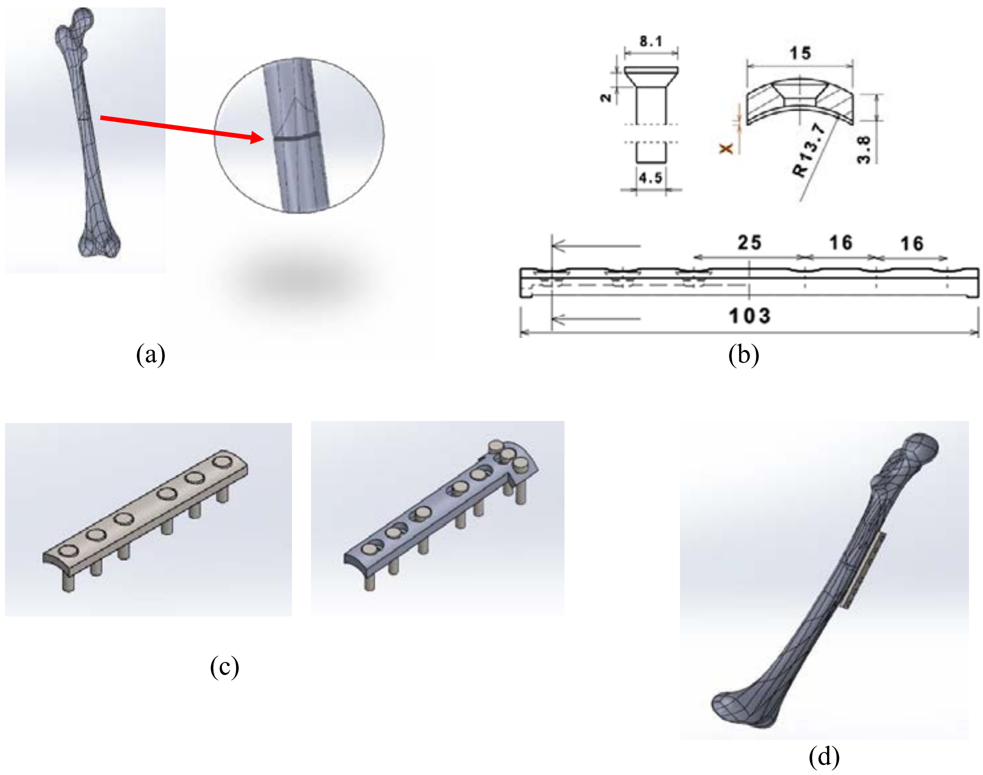

Figure 2: (a) Representation of Fracture (b) 4.5mm Bone Plate Dimension [39] (c) 4.5/5mm DCP and LCP (d) Assemble of Fractured Parts and Plates

2.1.4. Assemble of Fracture Bone and Plates

The fractured bone and fixation plate were brought into the SOLIDWORKS 2023 assembly environment, where precise mating conditions were applied to ensure proper alignment and interaction between the components. The assembly was carefully configured to create a fully constrained and anatomically accurate model, mimicking the real-world relationship between the bone and the plate. Once finalized (see Fig. 2), the assembly was exported in a compatible format for further analysis in ANSYS. There, finite element simulations were performed to assess the biomechanical performance of the model under different loading conditions.

2.2. Finite Element Analysis

To address most building challenges, Finite Element Analysis (FEA) has been integrated with various design software tools. ANSYS, a general-purpose FEA software developed by ANSYS, Inc., is widely used for simulating and analyzing structural, thermal, fluid, acoustic, and electromagnetic problems. It supports efficient design, modeling, optimization, and analysis through advanced Computer-Aided Design (CAD) integration. In this thesis the geometric model was created in SOLIDWORKS, tailored to meet the specific requirements of the analysis. This model was then imported into ANSYS for finite element simulations to assess stress and total deformation under defined conditions. The simulations were carried out using the Static Structural module in ANSYS, which is ideal for evaluating mechanical performance under static loads. To ensure the results were accurate and reliable, appropriate material properties were assigned to the model, and boundary conditions were carefully set. The analysis focused on key indicators such as von Mises stress and total deformation, which are crucial for evaluating the structural integrity and overall performance of the component. This methodical approach provides a detailed understanding of the mechanical behavior, enabling meaningful conclusions to be drawn.

2.2.1. Bone Material Selection

The femur, a long bone in the human body, consists of two types of bone: cortical (compact) and cancellous (trabecular). Cortical bone forms the dense outer layer and makes up about 80% of total bone mass [40]. For this study, the femur was simplified to consist only of cortical bone, modeled as a dense cylindrical structure with a central marrow cavity. This approach streamlines the geometry for computational efficiency while preserving key biomechanical properties for finite element analysis (FEA). As bone material properties are not included in the ANSYS engineering data library, a custom material dataset was created to accurately simulate the behavior of fractured bone. Key mechanical properties of cortical bone, such as density, Young's modulus, Poisson's ratio, and ultimate strength, were sourced from existing literature and incorporated into the material model. These essential properties, crucial for finite element analysis, are outlined in Table 1 for easy reference [41].

Property	Cortical Bone	Unit
Density (ρ)	1.8×10^3	kg/m^3
Young's Modulus (E)	17×10^9	Pa
Shear Modulus (G)	7×10^9	Pa
Poisson's Ratio (ν)	0.3	_
Ultimate Tensile Strength	150	MPa
Ultimate Compressive Strength	170	MPa

Table 1: Properties of Femur Cortical Bone

2.2.2. Bone Plate Materials Selection

This study evaluates the mechanical performance of bone plates fabricated from magnesium alloy and stainless steel, selected for their unique and complementary properties in orthopedic applications. Magnesium alloy, a lightweight and biodegradable material, has gained attention for its ability to promote bone regeneration while gradually degrading in vivo, thereby reducing the need for secondary surgeries. Its biocompatibility and favorable mechanical properties, closely resembling natural bone, make it an excellent candidate for temporary implants [4]. Conversely, stainless steel is a widely established material in orthopedics, known for its exceptional mechanical strength, durability, and resistance to corrosion under physiological conditions. Its affordability and ease of manufacturing further contribute to its extensive use in clinical settings [42]. To evaluate the suitability of these materials for bone plates, standard femur bone models will be developed and virtually fractured using SolidWorks. Custom-designed bone plates made from magnesium alloy and stainless steel was assembled with the femur using bone screws, enabling a comparative analysis of their structural and biomechanical performance. Their properties in ANSYS Engineering data source are given below (Table 2).

	Magnesium Alloy	Stainless Steel	Unit
Density	1800	7750	Kg/m^3
Young's Modulus	4.5x10	1.93x11	Pa
Poisson's Ratio	0.35	0.31	
Bulk Modulus	5x10	1.693x11	Pa
Shear Modulus	1.6667x10	7.3664x10	Pa

Tensile Yield Strength	1.93x8	2.07x8	Pa
Compressive Yield Strength	1.93x8	2.07x8	Pa
Tensile Ultimate Strength	2.55x8	5.86x8	Pa

Table 2: Properties of Bone Plate Materials

2.2.3. Geometry

Since the primary objective of this study is to evaluate the stress and deformation in the bone plate, the bone plate and screws were unified into a single part using the Boolean operation in ANSYS geometry to simplify the analysis. Subsequently, repair tools were employed to correct any damaged geometries, including edges and angles.

2.2.4. Meshing

The 3D models of bone plates were drawn and assembled with fractured bone in SOLIDWORKS. Then combined geometry was meshed in ANSYS. Its mesh size was 4 mm with body size 3 mm. The element number was 114684 and the number of nodes was 169117. Table 2 shows the maximum stress & deformation corresponding to mesh size and Fig. 3 shows the mesh dependency test. This fine mesh resolution enables precise analysis of structural behavior and performance under various conditions.

Mesh Size (mm)	Nodes	Elements	Max Stress (MPa)
7	151675	104868	92.16
6	161270	109866	98.22
5	164564	111830	94.88
4	169117	114684	108.93
3	179304	121377	101.98

Table 3: Mesh Size variation

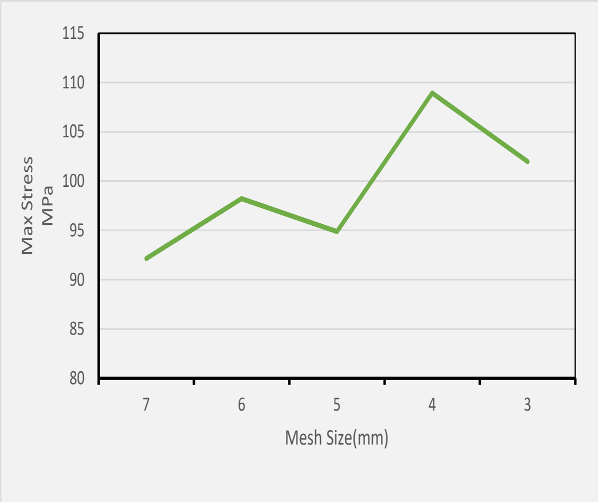

Figure 3: Mesh Dependency Curve

2.2.5. Boundary Condition (Force Analysis & Fixed Support)

In this study, the applied force was based on body weight, a key factor in defining boundary conditions for finite element analysis in ANSYS. A representative body weight of 70 kg (approximately 700 N) was chosen, reflecting the average weight of an adult in a normal standing posture. While body weight can vary depending on factors like age, gender, and physiological conditions, this standardization provides consistency and facilitates comparative analysis. This approach ensures reliable simulations while allowing flexibility for future studies to adapt the applied force to different scenarios as needed. The force calculation for normal standing condition is given in table below-

Healing Stage	**Force Range** (as % of Body Weight)	**Force Range (N)** (for a 70 kg person)
1. Inflammatory Stage	0–20%	0–140 N
2. Soft Callus Stage	20–50%	140–350 N
3. Hard Callus Stage	50–80%	350–560 N
4. Remodeling Stage	80–100%	560–700 N

Table 4: Force Analysis for 70kg Body Weight Patient

In the ANSYS simulation, boundary conditions were defined in two distinct regions to accurately represent physiological constraints. Fixed support conditions were applied to the lower segment of the femur (see Fig. 4) to simulate the natural immobilization of the bone during load-bearing. On the upper part of the femur, externally calculated forces representing physiological loads were applied (see Fig. 5) to mimic realistic stress conditions encountered during daily activities. This approach allowed for a more precise evaluation of the mechanical behavior of the bone-implant assembly under loading.

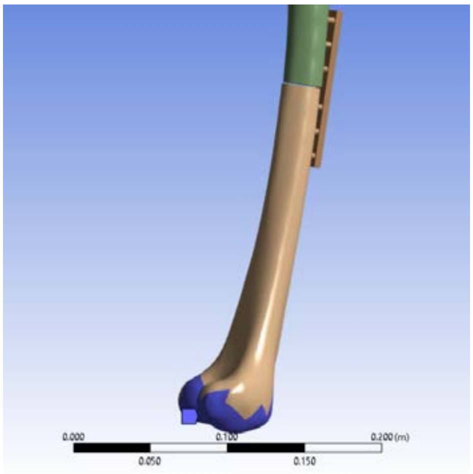

Figure 4: Fixed Support in Lower Part

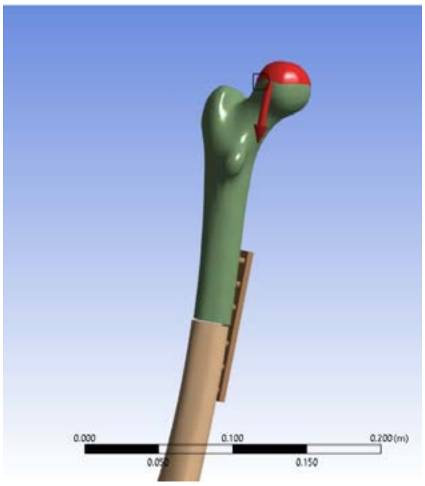

Figure 5: Force Applied in Upper Part

2.3. Simulated Data

This study presents a comparative finite element analysis (FEA) of two orthopedic fixation systems, Dynamic Compression Plate (DCP) and Locking Compression Plate (LCP), manufactured from stainless steel and magnesium alloy. The simulations were conducted under physiological loading conditions corresponding to four distinct stages of femoral fracture healing. Each healing stage exhibits a unique load-bearing capacity, expressed as a percentage of total body weight transmitted through the femur. For a 70 kg individual, these values were computed based on biomechanical data outlined in the preceding section and subsequently applied as input forces in ANSYS simulations. The primary objective was to evaluate stress distribution and deformation responses in each plate-material configuration, thereby providing insights into their mechanical performance and suitability across different healing phases.

2.3.1. Dynamic Compression Plate (DCP)

For the stainless steel DCP, four incremental loads ,140 N, 350 N, 560 N, and 700 N (Fig. 6-9), were applied to simulate progressive weight-bearing during femoral fracture healing. The finite element analysis revealed a proportional increase in von Mises stress and total deformation with rising load, indicating a linear elastic response within the studied range. All stress levels remained well below (Shown in Table-5) the ultimate tensile strength (UTS) of stainless steel, confirming its suitability for continuous load-bearing throughout the healing process.

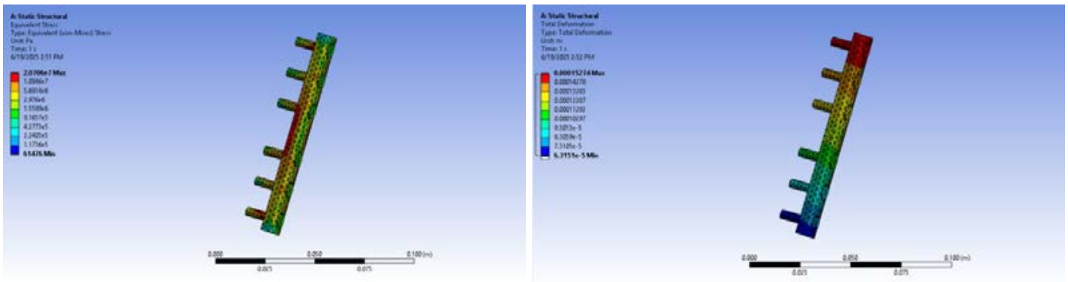

(a) (b)

Figure 6: (a) Equivalent Stress and (b) Total Deformation at 140N at DCP (SS) Bone plate

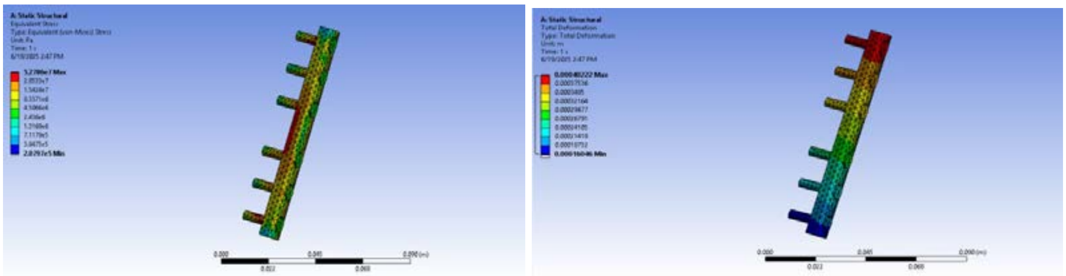

(a) (b)

Figure 7: (a) Equivalent Stress and (b) Total Deformation at 350N at DCP (SS) Bone plate

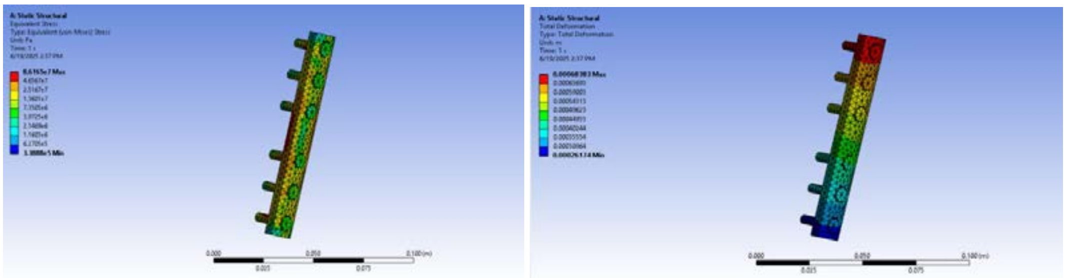

(a) (b)

Figure 8: (a) Equivalent Stress and (b) Total Deformation at 560N at DCP (SS) Bone plate.

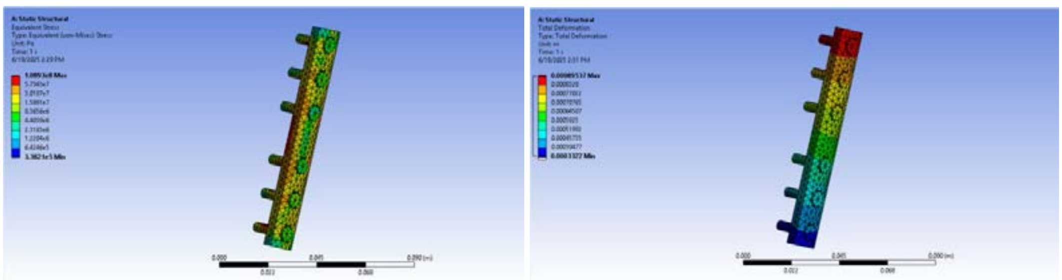

(a) (b)

Figure 9: (a) Equivalent Stress and (b) Total Deformation at 700N at DCP (SS) Bone plate

In contrast, the magnesium alloy DCP exhibited higher stress and deformation at all load levels due to its lower stiffness (**Fig. 10-13**). At 600 N, the induced stress (~272 MPa) exceeded the UTS of 250 MPa, indicating mechanical overload (**Shown in Table-5**). Under 700 N loading, the plate was predicted to fail, suggesting that magnesium alloy DCPs are unsuitable for high-load conditions during early and mid-stage healing.

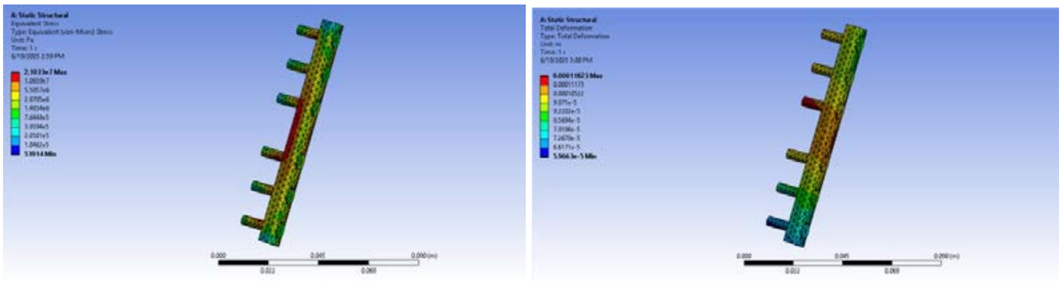

(a) (b)

Figure. 10: (a) Equivalent Stress and (b) Total Deformation at 140N at DCP (Mg Alloy) Bone plate

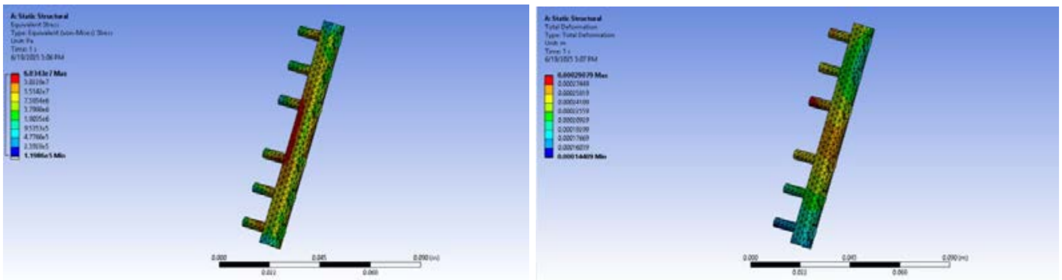

(a) (b)

Figure 11: (a) Equivalent Stress and (b) Total Deformation at 350N at DCP (Mg Alloy) Bone plate

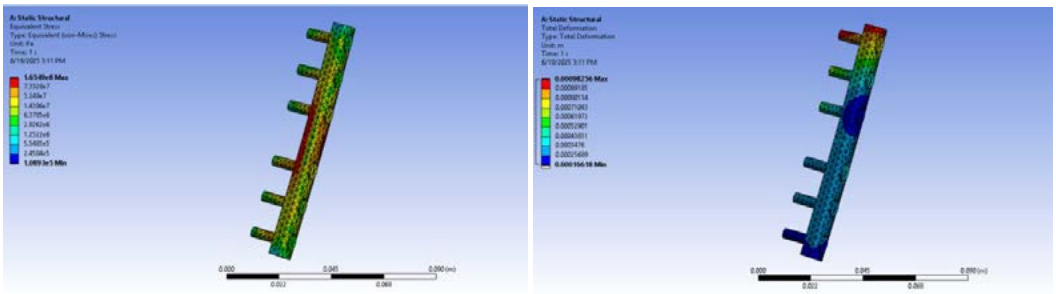

(a) (b)

Figure 12: (a) Equivalent Stress and (b) Total Deformation at 560N at DCP (Mg Alloy) Bone plate

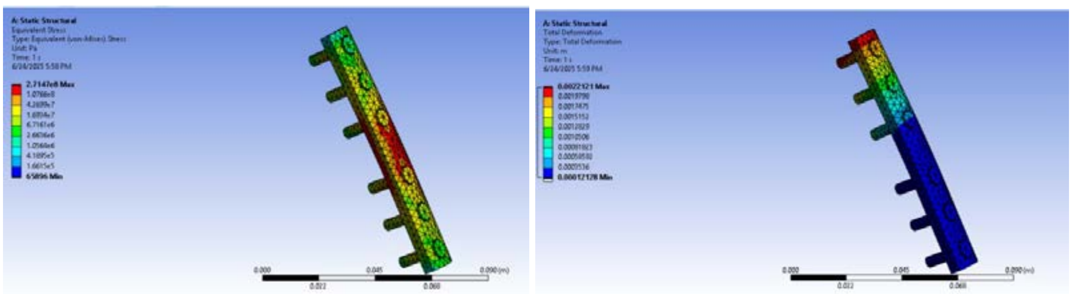

(a) (b)

Figure 13: (a) Equivalent Stress and (b) Total Deformation at 600N at DCP (Mg Alloy) Bone plate

		Stainless Steel		Magnesium Alloy	
Healing Stages	Maximum Force (N)	Max Equivalent Stress (MPa)	Max Total Deformation (m)	Max Equivalent Stress (MPa)	Max Total Deformation (m)
1. Inflammatory	140 N	20.71	1.527×10^{-4}	21.03	1.182×10^{-4}
2. Soft Callus	350 N	52.78	4.022×10^{-4}	60.34	2.907×10^{-4}
3. Hard Callus	560 N	86.16	6.838×10^{-4}	165.49	9.825×10^{-4}
4. Remodeling	700 N	108.93	8.953×10^{-4}	Greater than 250	70.034×10^{-4}

Table 5: Simulated Data for DCP Bone Plate

2.3.2. Locking Compression Plate (LCP)

When modeled with stainless steel, the LCP demonstrated stable performance under all four load stages (140 N, 350 N, 560 N, and 700 N) (Fig. 14-17), with stresses and deformations increasing proportionally but remaining well below (Shown in Table-6) the material's UTS.

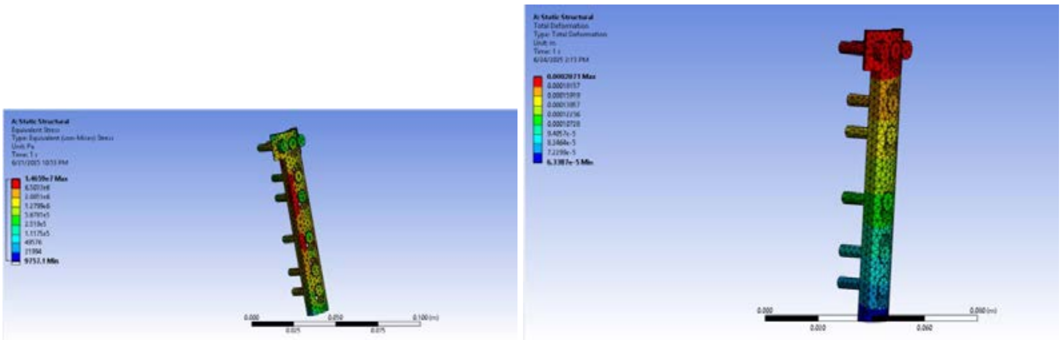

(a) (b)

Figure 14: (a) Equivalent Stress and (b) Total Deformation at 140N at LCP (SS) Bone plate

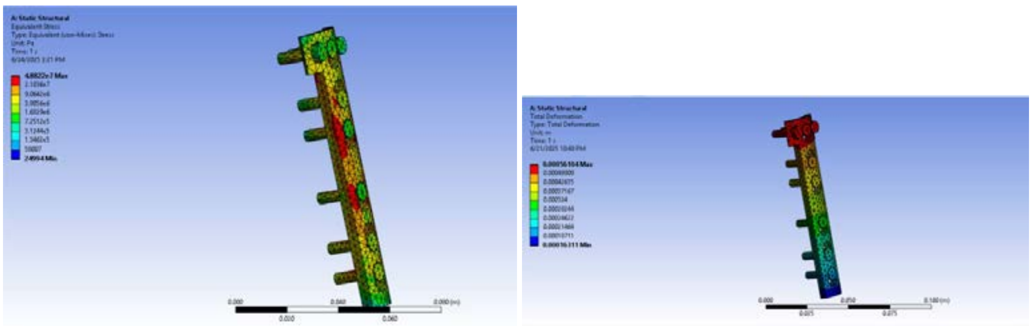

(a) (b)

Figure 15: (a) Equivalent Stress and (b) Total Deformation at 350N at LCP (SS) Bone plate

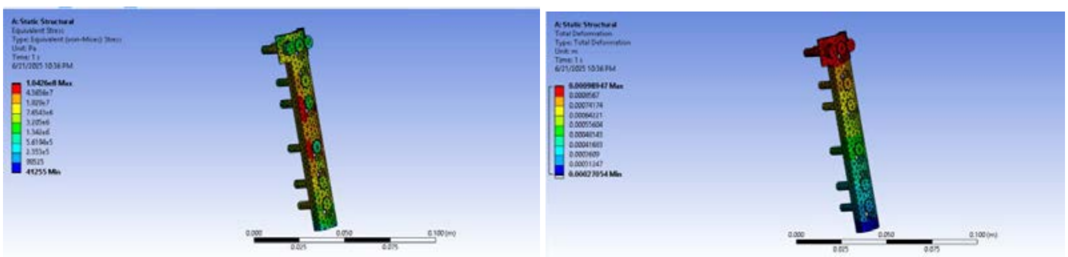

(a) (b)

Figure 16: (a) Equivalent Stress and (b) Total Deformation at 560N at LCP (SS) Bone plate

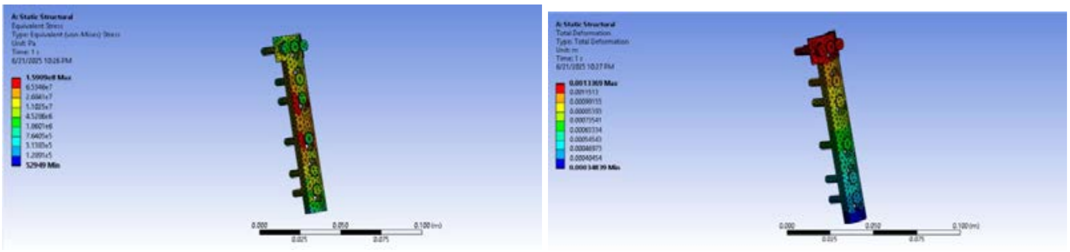

(a) (b)

Figure 17: (a) Equivalent Stress and (b) Total Deformation at 700N at LCP (SS) Bone plate

The magnesium alloy LCP, however, showed a different trend: at 430 N, the stress (~240 MPa) approached the UTS (**Fig. 18-20**), indicating a critical load threshold (**Shown in Table-6**). Loads of 560 N and 700 N were predicted to exceed the UTS, leading to probable structural failure. These findings suggest that while stainless steel LCPs can safely withstand full weight-bearing during all healing stages, magnesium alloy LCPs should be restricted to low-load conditions or early partial weight-bearing to avoid premature failure.

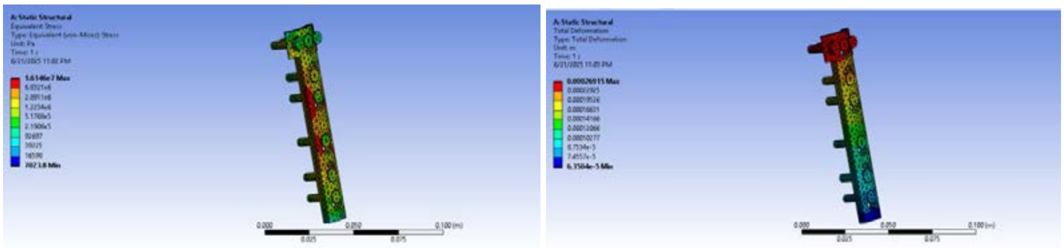

(a) (b)

Figure 18: (a) Equivalent Stress and (b) Total Deformation at 140N at LCP (Mg Alloy) Bone plate

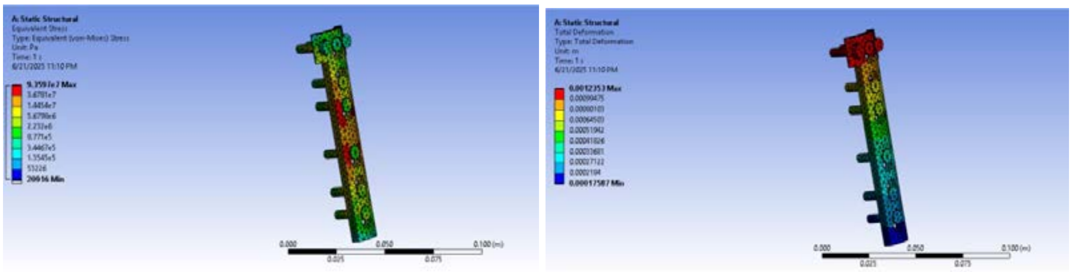

(a) (b)

Figure 19: (a) Equivalent Stress and (b) Total Deformation at 350N at LCP (Mg Alloy) Bone plate

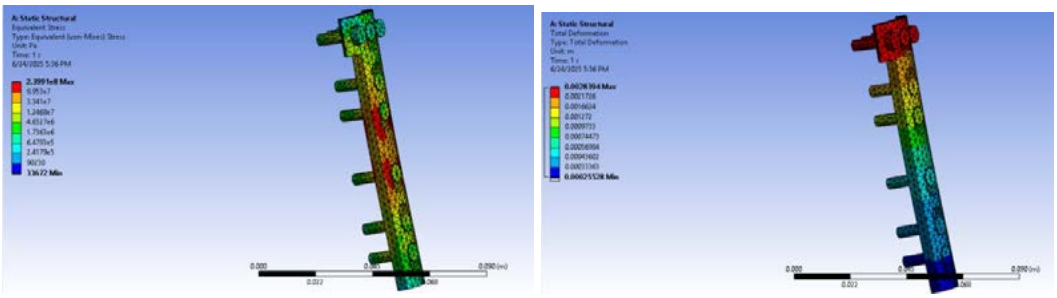

(a) (b)

Figure 20: (a) Equivalent Stress and (b) Total Deformation at 430N at LCP (Mg Alloy) Bone plate

Citation: Mesbah, M. M. T. I., Shahariar, M. D. T., Mamun, A. A. (2026). FEA Based Biomechanical Analysis of Stainless Steel and Magnesium Alloy Femur Bone Plates Under Healing-Stage Load Conditions. *J Appl Mech Rev Rep, 2*(2), 1-16.

		Stainless Steel		Magnesium Alloy	
Healing Stages	Maximum Force (N)	Max Equivalent Stress (MPa)	Max Total Deformation (m)	Max Equivalent Stress (MPa)	Max Total Deformation (m)
1. Inflammatory	140 N	14.65	2.071×10^{-4}	16.14	2.691×10^{-4}
2. Soft Callus	350 N	48.82	5.610×10^{-4}	93.59	12.353×10^{-4}
3. Hard Callus	560 N	104.26	9.894×10^{-4}	Greater than 250	15.442×10^{-4}
4. Remodeling	700 N	159.09	13.369×10^{-4}	Greater than 250	565.81×10^{-4}

Table 6: Simulated Data for LCP Bone Plate

3. Result and Discussion

3.1. Stainless Steel Bone Plate

The graph (See Fig. 21) depicts the stress response of a stainless-steel plate under increasing forces (140 N to 700 N). The stress values rise linearly from approximately 20 MPa at 140 N to 160 MPa at 700 N, indicating a consistent and predictable elastic behavior. Both DCP (Dynamic Compression Plate) and LCP (Locking Compression Plate) configurations follow a similar trend, suggesting that the plate's material properties dominate over the fixation method in stress distribution. The absence of a sharp yield point implies that the stainless steel remains within its elastic deformation range under these loading conditions. However, under heavy (560N & 700N) identical loading conditions, the Locking Compression Plate (LCP) exhibited higher stress concentrations compared to the Dynamic Compression Plate (DCP). Since lower stress levels in the fixation device are generally preferred to promote faster bone healing and reduce the risk of implant failure, the DCP demonstrates a more favorable biomechanical performance in this context. These results suggest that, for the specific loading scenarios analyzed, the DCP may offer advantages over the LCP in terms of stress distribution and overall structural efficiency.

In contrast to the magnesium alloy, the stainless-steel plate exhibits minimal deformation, with values peaking at only 0.0016 m even under the maximum load of 700 N (See Fig. 21). The deformation trend is nearly linear, reinforcing the material's high stiffness and elastic dominance. The DCP and LCP configurations show negligible variation, further confirming that stainless steel's rigidity is the primary factor in resisting deformation. This behavior makes it suitable for applications requiring dimensional stability under load.

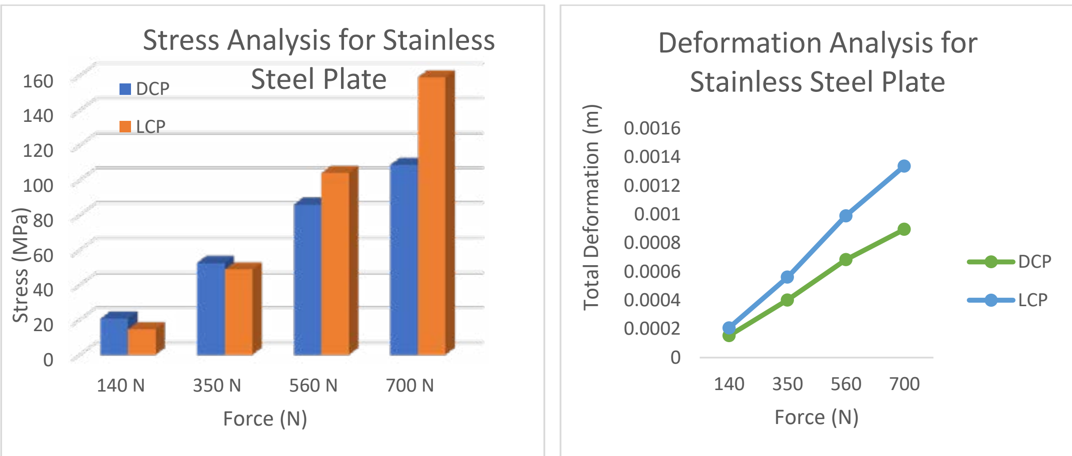

(a) Equivalent Stress DCP vs LCP **(b) Total Deformation DCP vs LCP**

Figure 21: Comparison Between Two Plates for Stainless Steel Materials

3.2. Magnesium Alloy Bone Plate

The stress response (See Fig. 22) of the magnesium alloy plate shows a steep increase, reaching up to 250 MPa at 700 N, significantly higher than stainless steel under the same load. The trend suggests that while magnesium alloy deforms more easily, it develops higher internal stresses, likely due to its lower modulus of elasticity. As a result, for DCP it exceeds threshold value of ultimate strength at 700N and for LCP at both 560N & 700N. The DCP and LCP configurations exhibit similar stress trends. The higher stress levels imply potential susceptibility to fatigue or failure at lower cycle counts compared to stainless steel, necessitating careful design considerations in load-bearing applications.

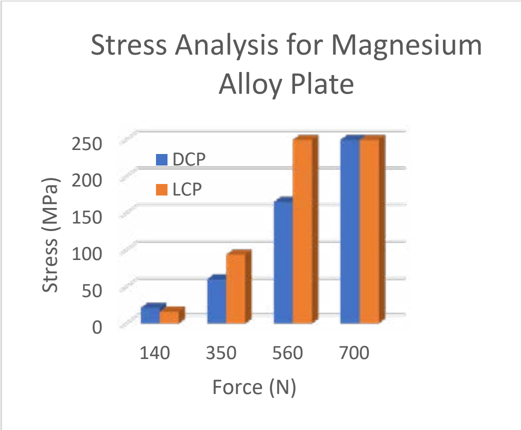

(a) Equivalent Stress DCP vs LCP.

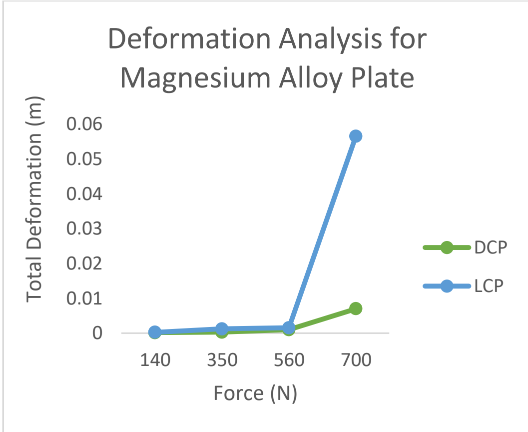

(b) Total Deformation DCP vs LCP

Figure 22: Comparison Between Two Plates for Magnesium Alloy Materials

The graph (See Fig. 22) illustrates the total deformation of a magnesium alloy plate under varying forces. The deformation increases nonlinearly, reaching up to 0.06 m at 700 N, which is significantly higher than that of stainless steel. The trend suggests that magnesium alloy undergoes substantial plastic deformation at higher loads, highlighting its ductility. The DCP and LCP configurations show minor differences, implying that deformation is primarily material-dependent rather than fixation-dependent. The nonlinearity may indicate work hardening or viscoelastic effects at higher strains. The numerical results obtained in this study were not directly validated against new experimental measurements. Instead, the reliability of the finite element model was assessed through mesh convergence analysis and by comparing the observed trends with previously published experimental and numerical studies. The finite element analysis (FEA) results indicate that stainless steel bone plates, in both Dynamic Compression Plate (DCP) and Locking Compression Plate (LCP) configurations, exhibit stable linear elastic behavior under all applied loading conditions up to 700 N. The maximum von Mises stress values remained significantly below the material's ultimate tensile strength (approximately 520 MPa), with peak stresses of about 108.93 MPa for DCP and 160 MPa for LCP at the highest load. These findings suggest that stainless steel plates operate safely within the elastic range and are suitable for load-bearing orthopedic applications. This observation is consistent with the findings of Amalraju and Shaik Dawood [25], who reported superior mechanical performance of stainless steel implants due to their high strength and low deformation characteristics. In contrast, the magnesium alloy plates showed a significant increase in stress and deformation with increasing load. The stress values approached or exceeded the material's ultimate tensile strength (approximately 250 MPa) at higher loads, indicating a high risk of mechanical failure under full weight-bearing conditions. For instance, stress levels reached approximately 272 MPa at 600 N in the DCP configuration and approached the material limit even at lower loads in the LCP configuration. These results agree with Wicaksono et al. [43], who observed elevated von Mises stress and deformation in magnesium alloy plates under similar loading conditions. Furthermore, the limitations of magnesium alloys in load-bearing orthopedic applications, particularly due to insufficient mechanical strength and rapid degradation, have been emphasized by Amukarimi et al. [44]. The progressive increase in stress and deformation with increasing load also follows biomechanical trends reported in earlier studies, such as Fouad (2011) [29], where increasing load levels led to higher stress concentration in bone-plate systems. Overall, the present results are consistent with established findings in the literature.

The mechanical performance of stainless steel and magnesium alloy bone plates under realistic loading conditions provides useful insight into their clinical applicability. Stainless steel plates, in both DCP and LCP configurations, showed stable elastic behavior across all loading levels. The maximum stress remained well below the material's ultimate tensile strength (~520 MPa), even at the highest load of 700 N, indicating a strong safety margin for full weight-bearing conditions in adult patients. In contrast, magnesium alloy plates exhibited much lower load tolerance. The DCP configuration approached failure at 560 N, while the LCP exceeded its strength limit (~250 MPa) at around 430 N. These findings are consistent with previous studies, which report that although magnesium alloys offer advantages such as biodegradability and better biomechanical compatibility, their limited strength restricts their use in high-load applications. Under lower loading conditions, representative of pediatric and adolescent body weights (approximately 20–55 kg), magnesium alloy plates may still be clinically viable. Their performance suggests potential suitability for early-stage healing or for patients with lower body weight. Therefore, while stainless steel remains the preferred choice for adult load-bearing fixation, magnesium alloys may serve as a promising alternative for temporary fixation in low-load scenarios.

4. Conclusion

This study presents a comparative finite element evaluation of DCP and LCP femur bone plates made from stainless steel and magnesium alloy under progressively increasing physiological loads. The results demonstrate that stainless steel plates provide stable mechanical performance, maintaining stress and deformation within safe limits up to 700 N, confirming their suitability for full weight-bearing applications. In contrast, magnesium alloy plates showed limited load-bearing capacity, with stress values approaching or exceeding material strength at higher loads. While this restricts their use in adult full-load conditions, their performance under lower loads suggests potential applicability in early-stage healing or in pediatric patients. The analysis also indicates that plate design influences performance, with DCP showing relatively lower stress levels than LCP under higher loads. A key contribution of this work is the use of a patient-specific femur model combined with load-based representation of healing progression, providing a practical framework for evaluating implant behavior under clinically relevant conditions. However, the study includes several limitations. The bone was modeled as homogeneous, screw geometry was not explicitly represented, and only static loading conditions were considered. These simplifications may influence the accuracy of the results. Overall, the findings emphasize the importance of material selection and plate design in orthopedic fixation and highlight the need for further research on improving the mechanical performance of biodegradable materials such as magnesium alloys for safe clinical use.

Author Contributions

1. M Tariqul Islam Mesbah: Conceptualization, Methodology, Writing – original draft, Investigation and analyses, Software, Validation.
2. Md Tanvir Shahariar: Data curation, Visualization, Validation.
3. Abdullah-Al-Mamun: Supervision, Resources, Validation, Writing – review & editing.
4. All authors have read and approved the final manuscript and agree to be accountable for all aspects of the work.

Competing Interests

The authors declare that they have no competing interests.

Funding

No funding was received for conducting this study.

Declaration of Generative AI use

During the preparation of this work, the authors used AI tools sometime to refine the language of the manuscript. All text, data analysis, and interpretations were independently produced and thoroughly verified by the authors.

Ethical Approval

This study did not involve human participants, animals, or clinical data directly. The femur models were collected from publicly available data for research purposes. Therefore, ethical approval and informed consent were not required.

References

1. Ferrucci, L., Baroni, M., Ranchelli, A., Lauretani, F., Maggio, M., Mecocci, P., & Ruggiero, C. (2014). Interaction between bone and muscle in older persons with mobility limitations. (19), 3178-3197.
2. Li, J., Qin, L., Yang, K., Ma, Z., Wang, Y., Cheng, L., & Zhao, D. (2020). Materials evolution of bone plates for internal fixation of bone fractures: A review. *Journal of Materials Science & Technology, 36,* 190-208.
3. Ayyappan, S. (2013). AO techniques of Dynamic Compression Plate (DCP) and Limited Contact Dynamic Compression Plate (LC–DCP) Application for Fracture Management in Dogs. *Advances in Animal and Veterinary Sciences, 1*(2S), 33-36.
4. “MedComm - 2021 - Amukarimi - Biodegradable magnesium-based biomaterials An overview of challenges and opportunities.pdf.”
5. “Fracture,” Physiopedia. Accessed: Dec. 30, 2024. [Online]. Available: https://www.physio-pedia.com/Fracture
6. “Bone Cortical And Cancellous,” Physiopedia. Accessed: Jan. 11, 2025. [Online]. Available: https://www.physio-pedia.com/Bone_Cortical_And_Cancellous
7. Maruyama, M., Rhee, C., Utsunomiya, T., Zhang, N., Ueno, M., Yao, Z., & Goodman, S. B. (2020). Modulation of the inflammatory response and bone healing. *Frontiers in endocrinology, 11,* 386.
8. “Ulna, articular, olecranon, simple - Plate with or without lag screw,” site name. Accessed: Jan. 14, 2025. [Online]. Available: https://surgeryreference.aofoundation.org/orthopedic-trauma/adult-trauma/proximal-forearm/basic-technique/ulna-articular-olecranon-simple-plate-with-or-without-lag-screw
9. “Snapshot.” Accessed: Dec. 27, 2024. [Online]. Available: https://www.physio-pedia.com/Femur
10. “Snapshot.” Accessed: Jan. 11, 2025. [Online]. Available: https://www.physio-pedia.com/Bone_Cortical_And_Cancellous
11. “Snapshot.” Accessed: Dec. 30, 2024. [Online]. Available: https://www.physio-pedia.com/Fracture
12. admin, “Orthopedic Plates - Types and Uses,” Siora Surgicals Private Limited. Accessed: Jan. 02, 2025. [Online]. Available: https://www.siiora.com/blogs/orthopedic-plates/
13. Ossiform, “Materials for Orthopedic Bone Reconstruction,” Ossiform - WE PRINT BONE. Accessed: Jan. 10, 2025. [Online]. Available: https://ossiform.com/materials-for-orthopedic-bone-reconstruction/
14. Maruyama, M., Rhee, C., Utsunomiya, T., Zhang, N., Ueno, M., Yao, Z., & Goodman, S. B. (2020). Modulation of the inflammatory response and bone healing. *Frontiers in endocrinology, 11,* 386.
15. “How Broken Bones Heal (for Parents).” Accessed: Jan.

14, 2025. [Online]. Available: https://kidshealth.org/en/parents/fractures-heal.html

16. "Plating," site name. Accessed: Jan. 02, 2025. [Online]. Available: https://surgeryreference.aofoundation.org/orthopedic-trauma/adult-trauma/basic-technique/basic-principles-of-plating
17. "Harasen - Orthopedic hardware and equipment for the beginner.pdf."
18. Uhthoff, H. K., Poitras, P., & Backman, D. S. (2006). Internal plate fixation of fractures: short history and recent developments. *Journal of orthopaedic science, 11*(2), 118-126.
19. Ahirwar, H., Gupta, V. K., & Nanda, H. S. (2021). Finite element analysis of fixed bone plates over fractured femur model. *Computer Methods in Biomechanics and Biomedical Engineering, 24*(15), 1742-1751.
20. Marco, M., Giner, E., Larrainzar-Garijo, R., Caeiro, J. R., & Miguélez, M. H. (2017). Numerical modelling of femur fracture and experimental validation using bone simulant. *Annals of biomedical engineering, 45*(10), 2395-2408.
21. Ganesh, V. K., Ramakrishna, K., & Ghista, D. N. (2005). Biomechanics of bone-fracture fixation by stiffness-graded plates in comparison with stainless-steel plates. *Biomedical engineering online, 4*(1), 46.
22. Kalaiyarasan, A., Sankar, K., & Sundaram, S. (2020). Finite element analysis and modeling of fractured femur bone. *Materials Today: Proceedings, 22,* 649-653.
23. Coquim, J., Clemenzi, J., Salahi, M., Sherif, A., Tavakkoli Avval, P., Shah, S., ... & Zdero, R. (2018). Biomechanical analysis using FEA and experiments of metal plate and bone strut repair of a femur midshaft segmental defect. *BioMed research international, 2018*(1), 4650308.
24. Bagheri, Z. S., Tavakkoli Avval, P., Bougherara, H., Aziz, M. S., Schemitsch, E. H., & Zdero, R. (2014). Biomechanical analysis of a new carbon fiber/flax/epoxy bone fracture plate shows less stress shielding compared to a standard clinical metal plate. *Journal of biomechanical engineering, 136*(9), 091002.
25. Amalraju, D., & Dawood, A. S. (2012). Mechanical strength evaluation analysis of stainless steel and titanium locking plate for femur bone fracture. *Engineering Science and Technology: An International Journal, 2*(3), 381-388.
26. Dhanopia, A., & Bhargava, M. (2017). Finite element analysis of human fractured femur bone implantation with PMMA thermoplastic prosthetic plate. *Procedia engineering, 173,* 1658-1665.
27. Sankar, K., Kalaiyarasan, A., Sasikala, D., Selvarasu, S., Rangarajan, J., Kirubakaran, J., & Vijayakumar, R. (2023). Finite Element Analysis of Fractured Femur Bone with Prosthetic Bone Plates Using ANSYS Software. *Cardiometry,* (26), 544-549.
28. Satapathy, P. K., Sahoo, B., Panda, L. N., & Das, S. (2018, March). Finite element analysis of functionally graded bone plate at femur bone fracture site. In *IOP conference series: materials science and engineering* (Vol. 330, No. 1, p. 012027). IOP Publishing.
29. Fouad, H. J. M. E. (2011). Assessment of function-graded materials as fracture fixation bone-plates under combined loading conditions using finite element modelling. *Medical Engineering & Physics, 33*(4), 456-463.
30. Guo, Z., Liu, H., Luo, D., Cai, T., Zhang, J., & Wu, J. (2023). Application of Cortical Bone Plate Allografts Combined with Less Invasive Stabilization System (LISS) Plates in Fixation of Comminuted Distal Femur Fractures. *Medicina, 59*(2), 207.
31. Ferrucci, L., Baroni, M., Ranchelli, A., Lauretani, F., Maggio, M., Mecocci, P., & Ruggiero, C. (2014). Interaction between bone and muscle in older persons with mobility limitations. *Current pharmaceutical design, 20*(19), 3178-3197.
32. Li, J., Qin, L., Yang, K., Ma, Z., Wang, Y., Cheng, L., & Zhao, D. (2020). Materials evolution of bone plates for internal fixation of bone fractures: A review. *Journal of Materials Science & Technology, 36,* 190-208.
33. Mehboob, A., Mehboob, H., & Chang, S. H. (2020). Evaluation of unidirectional BGF/PLA and Mg/PLA biodegradable composites bone plates-scaffolds assembly for critical segmental fractures healing. Composites Part *A: Applied Science and Manufacturing, 135,* 105929.
34. Alaneme, K. K., Kareem, S. A., Olajide, J. L., Sadiku, R. E., & Bodunrin, M. O. (2022). Computational biomechanical and biodegradation integrity assessment of Mg-based biomedical devices for cardiovascular and orthopedic applications: A review. *International Journal of Lightweight Materials and Manufacture, 5*(2), 251-266.
35. Wicaksono, M. A., Suharno, B., Astuti, W., Sumardi, S., Supriyatna, Y. I., Ulfah, I. M., ... & Sugiyanto. (2025). Biodegradable innovation: investigating static structural properties of AZ31B magnesium based on experimental and finite element analysis. *International Journal on Interactive Design and Manufacturing (IJIDeM), 19*(6), 4013-4024.
36. Liebl, H., Garcia, E. G., Holzner, F., Noel, P. B., Burgkart, R., Rummeny, E. J., ... & Bauer, J. S. (2015). In-vivo assessment of femoral bone strength using Finite Element Analysis (FEA) based on routine MDCT imaging: a preliminary study on patients with vertebral fractures. *PloS one, 10*(2), e0116907.
37. "femur bone - Recent models | 3D CAD Model Collection | GrabCAD Community Library." Accessed: Jan. 20, 2025. [Online]. Available: https://grabcad.com/library?page=1&time=all_time&sort=recent&query=femur%20bone
38. Meeson, R., Moazen, M., Sanghani-Kerai, A., Osagie-Clouard, L., Coathup, M., & Blunn, G. (2019). The influence of gap size on the development of fracture union with a micro external fixator. *Journal of the Mechanical Behavior of Biomedical Materials, 99,* 161-168.
39. Fouda, N., Mostafa, R., & Saker, A. (2019). Numerical study of stress shielding reduction at fractured bone using metallic and composite bone-plate models. *Ain Shams Engineering Journal, 10*(3), 481-488.
40. "Structure and composition of bone." Accessed: Jan. 21, 2025. [Online]. Available: https://www.doitpoms.ac.uk/tlplib/bones/structure.php
41. Reddy, M. K., Ganesh, B. K. C., Bharathi, K. C. K., & ChittiBabu, P. (2016). Use of finite element analysis

to predict type of bone fractures and fracture risks in Femur due to Osteoporosis. *Journal of Osteoporosis and Physical Activity, 4*(3), 1-8.

42. "Commonly Used Plates and Screws | Cave Veterinary Specialists." Accessed: Dec. 30, 2024. [Online]. Available: https://www.cave-vet-specialists.co.uk/veterinary-professionals/tips-from-our-experts/commonly-used-plates-and-screws
43. Wicaksono, M. A., Sukmana, I., Riszal, A., Hendronursito, Y., Nazarrudin, R., & Haviz, M. (2024). Comparison study between the experimental and finite element analysis (FEA) on a static load of magnesium AZ31B as biodegradable bone plate material. *Journal of Innovation and Technology, 5*(2), 62-68.
44. Amukarimi, S., & Mozafari, M. (2022). Biodegradable magnesium biomaterials—road to the clinic. *Bioengineering, 9*(3), 107.